Chaos bound for spinning particles: violation in Kerr black holes

Chuanhong Gao (高钏泓)[1,2†] Tetvui Chong[2‡]

[1]Sichuan Technology and Business University, Chengdu 611745, China
[2]Faculty of Engineering and Quantity Surveying, INTI International University, Nilai 71800, Malaysia

Abstract: In this work, we investigate the Lyapunov exponents that characterize the chaotic dynamics of neutral spinning particles around a Kerr black hole and perform a stringent test of the chaos bound in this framework. We carry out a systematic analysis of the dependence of these exponents on the black hole angular momentum, the particle spin, and its total angular momentum. For a non-extremal Kerr black hole with rotational parameter $a = \pm 0.90$, no violation of the chaos bound is observed when the black hole rotation is aligned with the z-axis. In the anti-aligned configuration, violations occur only when the particle spin magnitude or total angular momentum exceeds a critical threshold. In the extremal case, which corresponds to a zero-temperature thermal state, the surface gravity vanishes. Within the parameter ranges for which unstable equilibrium orbits exist, the exponents are found to be positive. These results provide clear evidence of violation of the bound by a spinning particle in Kerr spacetime.

Keywords: neutral spinning particle, Lyapunov exponents, chaos bound

DOI: 10.1088/1674-1137/ae9b89 **CSTR:** 32044.14.ChinesePhysicsC.50115115

I. INTRODUCTION

Chaos is an important phenomenon in nonlinear dynamical systems and is characterized by extreme sensitivity to initial conditions. The Lyapunov exponent (LE), which quantifies this sensitivity, serves as a key diagnostic for characterizing chaos. In classical systems, the exponent is explicitly defined by the exponential growth rate of infinitesimal perturbations along particle trajectories. In quantum systems, however, where well-defined trajectories are absent, the exponent must be inferred from quantum probes such as out-of-time-ordered correlators (OTOCs), which capture the scrambling of quantum information [1−4]. In a seminal work, Maldacena, Shenker, and Stanford conjectured that, in thermal quantum systems with a large number of degrees of freedom, the exponent is constrained by a universal upper bound (the chaos bound) [5],

$$\lambda \leq \frac{2\pi k_B T}{\hbar}, \tag{1}$$

where T denotes the temperature of the system, and k_B and $\hbar$ are the Boltzmann constant and the reduced Planck constant, respectively. This conjecture has profound implications for black hole physics and holographic duality and has garnered widespread support within the research community [6−12]. Notably, the investigation of the butterfly velocity by Shenker and Stanford [13] provides a prominent example, in which an analysis of holographic duality and chaotic dynamics reveals a direct relationship between the exponent and the black hole temperature. Further support is provided by studies of the Sachdev–Ye–Kitaev (SYK) model [14−17], which exhibits maximal chaotic behavior, with its Lyapunov exponent saturating the chaos bound and thereby supporting its validity.

In the classical black hole context, Hashimoto and Tanahashi [18] demonstrated that the Lyapunov exponent is independent of both the type of external force and the particle mass, and that it is bounded above by the surface gravity κ of the horizon, as expressed by the inequality

$$\lambda \leq \kappa. \tag{2}$$

By exploiting the thermodynamic relation between surface gravity and temperature, this result is consistent with the conjectured MSS bound and suggests a universal behavior spanning both the classical and quantum regimes.

However, subsequent studies revealed that this bound can be violated. When charged particles orbit charged black holes, electromagnetic interactions make it possible to tune the charge-to-mass ratio of the particles so that they approach the event horizon of the black hole. On this basis, Zhao et al. investigated chaos bounds for charged particles around various charged black holes and

Received 19 May 2026; Accepted 17 August 2026; Accepted manuscript online 18 August 2026
† E-mail: chuanhonggao@hotmail.com (Corresponding author)
‡ E-mail: chongtetvui@gmail.com
©2026 Chinese Physical Society and the Institute of High Energy Physics of the Chinese Academy of Sciences and the Institute of Modern Physics of the Chinese Academy of Sciences and IOP Publishing Ltd. All rights, including for text and data mining, AI training, and similar technologies, are reserved.

found that the exponents for particles in Reissner–Nordström (RN) and Reissner–Nordström anti-de Sitter (RN-AdS) spacetimes satisfy the bound, whereas violations occur for other black holes [19]. Notably, their study did not account for the effect of particle angular momentum on the exponents. By incorporating this effect, Lei and Ge reexamined the bounds for charged particles around RN and RN-AdS black holes and found that the bound is also violated [20]. Such violations have also been observed in other spherically symmetric spacetimes [21−24], as well as in axisymmetric spacetimes, including Kerr-Newman [25], Kerr-Newman-AdS black holes [26], and other axisymmetric black holes [27−29]. Additional examples of such violations are reported in [30−36].

It is noteworthy that the aforementioned studies focus primarily on charged particles outside black holes, whereas investigations of neutral spinning particles remain comparatively limited. Moreover, although the orbital motion of spinning particles around black holes has been widely studied, the impact of particle spin on the chaos bound has received little dedicated attention, with the notable exception of Ref. [37]. As shown in that work, violations of the chaos bound do not occur as long as the charge of the RN black hole remains below a threshold value, irrespective of the particle's spin magnitude and total angular momentum. This finding highlights the pivotal role of the black hole charge in triggering violations of the bound. More recently, Ref. [38] extended the study of spinning particles to the Einstein-Euler-Heisenberg-AdS spacetime and found violations of the chaos bound in that background as well.

In this work, we investigate the LEs characterizing the chaotic motion of neutral spinning particles in Kerr black hole spacetime, with the aim of assessing the applicability of the chaos bound conjecture in this context. The centrifugal force provides the support required for the particle's orbital equilibrium. The black hole angular momentum, the particle spin magnitude, and the particle's total angular momentum are identified as the key parameters governing these exponents. By evaluating the exponents for specific combinations of these parameters, we seek to determine whether the chaos bound holds. In our analysis, we systematically consider configurations in which the black hole rotation is either parallel or antiparallel to the z-axis, together with cases in which the particle spin is aligned or anti-aligned with the z-axis. Notably, for the extremal black hole case—which corresponds to a zero-temperature thermal state—we further test the validity of the bound under this limiting condition.

The remainder of this paper is organized as follows. In Sec. II, we review the motion of a spinning particle orbiting a Kerr black hole and derive the radial equation of motion. In Sec. III, we analyze the influence of the particle spin, its total angular momentum, and the black hole angular momentum on the LEs, and subject the chaos bound to a detailed examination. The final section is devoted to our conclusions and discussions.

II. MOTIONS OF SPINNING PARTICLES AROUND KERR BLACK HOLE

In this section, we review the motion of a spinning particle in Kerr black hole spacetime, a vacuum solution of Einstein's field equations that describes a rotating gravitational field. In Boyer–Lindquist coordinates, the Kerr metric is given by

$$\begin{aligned} \mathrm{d}s^2 =& -\left(1-\frac{2Mr}{\Sigma}\right)\mathrm{d}t^2 - \frac{4Mar\sin^2\theta}{\Sigma}\mathrm{d}t\mathrm{d}\varphi + \frac{\Sigma}{\Delta}\mathrm{d}r^2 + \Sigma\mathrm{d}\theta^2 \\ &+ \left(r^2+a^2+\frac{2Mra^2\sin^2\theta}{\Sigma}\right)\sin^2\theta\mathrm{d}\varphi^2, \end{aligned} \tag{3}$$

where $\Delta = r^2 - 2Mr + a^2$ and $\Sigma = r^2 + a^2\cos^2\theta$. The parameters M and a denote the black hole mass and rotation parameter, respectively. The total angular momentum of the black hole is $J_{\mathrm{BH}} = Ma$, with $a > 0$ ($a < 0$) corresponding to rotation about the z-axis in the positive (negative) direction. The equation $\Delta = 0$ has two roots, $r_\pm = M \pm \sqrt{M^2 - a^2}$, corresponding to the event horizon at r_+ and the inner horizon at r_-. The surface gravity of the black hole is given by

$$\kappa = \frac{\sqrt{M^2-a^2}}{2Mr_+}. \tag{4}$$

In the extremal limit, the inner and outer horizons coincide, yielding $M = |a|$ for the mass and angular momentum parameters. Under this condition, the surface gravity vanishes identically, and the black hole becomes a zero-temperature thermodynamic system.

The motion of a spinning test particle is governed by the Mathisson–Papapetrou–Dixon (MPD) equations [39]

$$\frac{Dp^\mu}{D\tau} = -\frac{1}{2}R^\mu_{\nu\alpha\beta}u^\nu S^{\alpha\beta}, \tag{5}$$

$$\frac{DS^{\mu\nu}}{D\tau} = p^\mu u^\nu - u^\mu p^\nu, \tag{6}$$

where $\frac{D}{D\tau}$ denotes the covariant derivative along the particle trajectory, and τ is an affine parameter of the orbit. $R^\mu_{\nu\alpha\beta}$ is the Riemann tensor, and $S^{\alpha\beta}$ denotes the spin tensor. p^μ and u^ν are the particle's four-momentum and four-velocity, respectively. However, the above two equations are incomplete because they do not specify the

representative point on the test particle used to define the spin and the trajectory. To establish the relationship between the particle's four-velocity and four-momentum precisely, the Tulczyjew-Dixon spin supplementary condition (TDSSC) is introduced [40, 41]

$$p_\mu S^{\mu\nu} = 0. \tag{7}$$

The 4-momentum and spin tensor correspond to two conserved quantities that characterize the test particle: its mass and the magnitude of its spin. They are expressed as follows

$$m^2 = -p^\mu p_\mu, \tag{8}$$

$$2S^2 = 2m^2\bar{s}^2 = S^{\mu\nu}S_{\mu\nu}. \tag{9}$$

Here, $\bar{s} = S/m$ denotes the particle's specific spin angular momentum. We set $s = \pm\bar{s}$ to enable a systematic study of two distinct physical configurations: (1) the case $s > 0$, corresponding to spin aligned with the z-axis, and (2) the case $s < 0$, corresponding to spin anti-aligned with the z-axis [42].

In Kerr spacetime, there are two Killing vectors, namely $\left(\frac{\partial}{\partial t}\right)^a$ and $\left(\frac{\partial}{\partial \varphi}\right)^a$. The first Killing vector is associated with a conserved energy $\bar{E}$,

$$\bar{E} = Em = -p_t + \frac{1}{2}g_{t\mu,\nu}S^{\mu\nu}. \tag{10}$$

The Killing vector $\left(\frac{\partial}{\partial \varphi}\right)^a$ is associated with the total angular momentum $\bar{J}$, which is oriented along the z-axis.

$$\bar{J} = Jm = p_\varphi - \frac{1}{2}g_{\varphi\mu,\nu}S^{\mu\nu}. \tag{11}$$

Restricting our analysis to equatorial orbits of spinning particles around a Kerr black hole, we solve the equations of motion using the MPD equations in conjunction with the TDSSC. The dynamics of spinning test particles in Kerr spacetime have been extensively investigated in several foundational works [43–48]. In the seminal paper by Saijo *et al*. [49], the equations of motion for the spacetime coordinates r, t, and φ were derived as follows:

$$\Sigma_s\Lambda_s\frac{\mathrm{d}t}{\mathrm{d}\tau} = a\left(1+\frac{3Ms^2}{r\Sigma_s}\right)[J-(a+s)E] + \frac{r^2+a^2}{\Delta}P_s, \tag{12}$$

$$\Sigma_s\Lambda_s\frac{\mathrm{d}\varphi}{\mathrm{d}\tau} = \left(1+\frac{3Ms^2}{r\Sigma_s}\right)[J-(a+s)E] + \frac{a}{\Delta}P_s, \tag{13}$$

$$\Sigma_s\Lambda_s\frac{\mathrm{d}r}{\mathrm{d}\tau} = \pm\sqrt{R_s}, \tag{14}$$

where

$$\Sigma_s = r^2\left(1-\frac{Ms^2}{r^3}\right), \tag{15}$$

$$\Lambda_s = 1 - \frac{3Ms^2r\left[-(a+s)E+J\right]^2}{\Sigma_s^3}, \tag{16}$$

$$R_s = P_s^2 - \Delta\left\{\frac{\Sigma_s^2}{r^2} + \left[-(a+s)E+J\right]^2\right\}, \tag{17}$$

$$P_s = \left[r^2+a^2+\frac{as(r+M)}{r}\right]E - \left(a+\frac{Ms}{r}\right)J. \tag{18}$$

To facilitate the subsequent computation of the exponent, we derive the time derivative of the radial coordinate. Using Eqs. (12) and (14), we obtain

$$\dot{r} = \frac{\mathrm{d}r}{\mathrm{d}t} = \frac{\pm\sqrt{R_s}}{a\left(1+\frac{3Ms^2}{r\Sigma_s}\right)[J-(a+s)E] + \frac{r^2+a^2}{\Delta}P_s}. \tag{19}$$

Here, the ± signs indicate the direction of the particle's radial motion: the positive sign corresponds to outward radial motion, whereas the negative sign corresponds to inward radial motion. Since our primary focus is the particle's dynamics in radial phase space, the expression for the derivative of the radial coordinate with respect to the azimuthal angle φ is omitted. The derivation of the above equation is based on the following assumptions: the characteristic radius of the spinning particle is much smaller than the curvature scale of the background spacetime, and the mass of the spinning body is much smaller than that of the black hole [49–51].

In the spinless limit ($s = 0$), the spin-curvature coupling vanishes, and the above equations reduce to the geodesic motion of a spinless test particle in the equatorial plane of Kerr spacetime. In this limit, one obtains

$$\Sigma_s\frac{\mathrm{d}t}{\mathrm{d}\tau} = a(J-aE) + \frac{r^2+a^2}{\Delta}P_s, \tag{20}$$

$$\Sigma_s\frac{\mathrm{d}\varphi}{\mathrm{d}\tau} = (J-aE) + \frac{a}{\Delta}P_s, \tag{21}$$

$$\Sigma_s \frac{\mathrm{d}r}{\mathrm{d}\tau} = \pm \sqrt{R_s}. \tag{22}$$

where

$$\Sigma_s = r^2, \tag{23}$$

$$\Lambda_s = 1, \tag{24}$$

$$P_s = E\left(r^2 + a^2\right) - aJ, \tag{25}$$

$$R_s = \left[E\left(r^2 + a^2\right) - aJ\right]^2 - \Delta\left[r^2 + (J - aE)^2\right]. \tag{26}$$

This is the standard radial potential for a massive spinless particle in Kerr spacetime. Therefore, the case $s = 0$ provides a consistency check for the present formalism and serves as the baseline for identifying the effects of particle spin [52]. This analytical reduction confirms the consistency of the equations of motion. A quantitative comparison with the known extremal Kerr geodesic result is presented in Sec. III.C.

III. EXAMINATION OF CHAOS BOUND

In this section, we conduct numerical investigations to assess the validity of the bound by analyzing the equatorial orbital dynamics of a spinning test particle around a Kerr black hole. Two spin configurations are considered: $s > 0$, corresponding to spin aligned with the z-axis, and $s < 0$, corresponding to spin anti-aligned with this axis.

A. LE

The particle's dynamics can be characterized by analyzing its radial effective potential, which governs orbital stability and is closely related to the LE. Previous work has established that the exponent is determined by the second radial derivative of the effective potential [53]. Here, we derive the exponent that characterizes the chaotic motion of a spinning test particle. We begin by considering the particle's motion,

$$\frac{1}{2} m\dot{r}^2 + V_{\mathrm{eff}} = 0. \tag{27}$$

For motion near an equilibrium orbit, the radial coordinate can be written as $r(t) = r_0 + \epsilon(t)$, where r_0 denotes the radius of the unstable orbit. Substituting this expression into Eq. (27) and performing a Taylor expansion yields

$$\frac{1}{2}\left(m\left(\frac{\mathrm{d}\epsilon}{\mathrm{d}t}\right)^2 + V''_{\mathrm{eff}}(r_0)\epsilon^2\right) + V_{\mathrm{eff}}(r_0) + O(\epsilon) \simeq 0, \tag{28}$$

In the above equation, $\epsilon = \epsilon(t)$, and $O(\epsilon)$ denotes the higher-order terms with respect to ϵ. By neglecting the higher-order and constant terms, it is straightforward to see that the coefficient of ϵ^2 corresponds to the LE [32, 54]

$$\lambda^2 = -\frac{V''_{\mathrm{eff}}(r_0)}{m}, \tag{29}$$

where λ denotes the exponent. By solving Eq. (27), the effective potential can be expressed in terms of the radial equation of motion as $V_{\mathrm{eff}}(r_0) = -\frac{1}{2}m\dot{r}^2$. Substituting this expression into the above equation, the exponent can be rewritten as

$$\lambda^2 = \frac{1}{2}\left.\frac{\mathrm{d}\dot{r}^2}{\mathrm{d}r^2}\right|_{r=r_0}. \tag{30}$$

It is evident that the value on the right-hand side of the equation can be positive, negative, or zero. Specifically, negative values indicate convergence of the radial motion, whereas positive values correspond to divergent behavior [19]. In the case of a positive value, even infinitesimal perturbations undergo exponential amplification, thereby indicating the presence of chaotic dynamics. The present study aims to explore the relationship between the exponent and the chaos bound.

B. Chaos bound in non-extremal Kerr spacetime

We now proceed to numerically calculate the exponent characterizing the chaos of the spinning particle and the surface gravity of the Kerr black hole. This is achieved by adopting specific values for the parameters associated with the black hole and the particle. In the numerical calculations, we set the black hole mass to $M = 1$. This choice fixes the length scale of the system, and all parameters are given in units of M. Subsequently, through a comparative analysis of the magnitudes of these two calculated quantities, we aim to test the chaos bound.

It is essential to accurately identify the unstable equilibrium orbits of the particle. These orbits are determined by the conditions $V_{\mathrm{eff}}(r_0) = V'_{\mathrm{eff}}(r_0) = 0$ and $V''_{\mathrm{eff}}(r_0) < 0$. In Fig. 1, we present the effective potential as a function of the radial coordinate. As shown, when the spin is parallel to the z-axis, increasing the spin magnitude shifts the radial position of the maximum of the effective potential to smaller radii, indicating that the unstable equilibrium orbit moves closer to the event horizon and thereby reducing the separation between the orbit and the horizon. Conversely, when the spin is antiparallel to the z-axis, increasing the spin magnitude shifts the unstable equilibri-

um orbit to larger radii, moving it farther from the horizon. These results demonstrate that the particle spin plays a crucial role in determining the location of the unstable orbit. In particular, the curve with $s=0$ corresponds to the spinless limit and serves as a reference case. For fixed values of the black hole spin parameter and the particle's conserved quantities, the deviations of the $s\neq 0$ curves from this reference case show how spin-curvature coupling modifies the effective potential and the corresponding unstable equilibrium orbit.

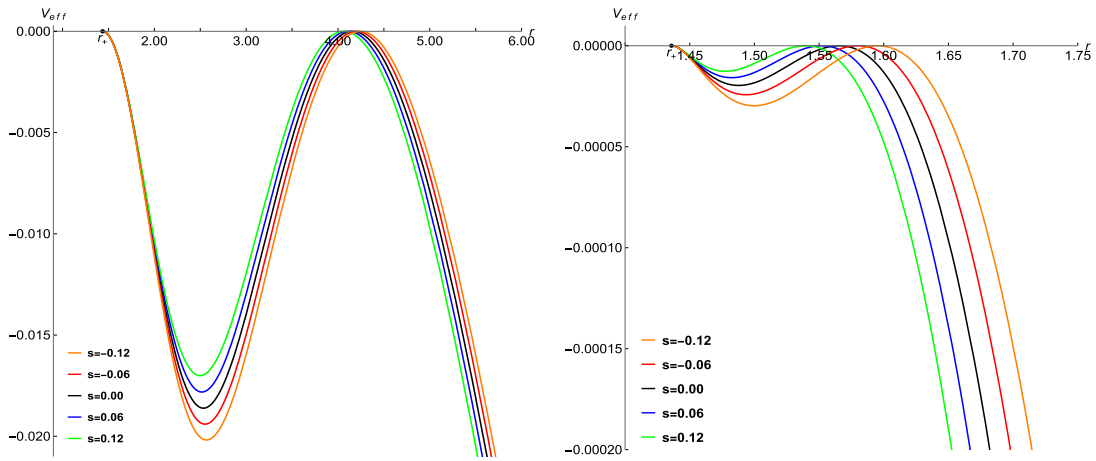
We compute the surface gravity and the exponent using Eqs. (4), (15), (17), (18), (19), and (30). The resulting dependence of the exponent on the particle spin, total angular momentum, and black hole angular momentum is illustrated in Figs. 2–5.

Figures 2 and 3 illustrate the influence of particle spin on the exponents, with curves of different colors corresponding to the particle's total angular momentum, $J=7,9,11,13$. We consider two configurations: the black hole rotating in the same direction as the z-axis ($a>0$) and in the opposite direction ($a<0$), as shown in Figs. 2 and 3, respectively. The surface gravity is $\kappa=0.1517839$.

As shown in Fig. 2, for a fixed total angular momentum, the exponents exhibit an approximately symmetric distribution with respect to particle spin, attaining their minimum near a slightly negative spin value. Regardless of whether the spin is parallel or antiparallel to the z-axis, the exponents increase monotonically with spin magnitude, indicating that a larger spin amplitude enhances the chaotic motion of the particle. Nevertheless, for all spin values considered, the exponents remain below the surface gravity, and the bound is not violated. For a fixed spin, the exponents increase with total angular momentum.

Figure 3 presents the case in which the black hole rotates opposite to the z-axis ($a<0$). Here, the trend of the curves changes significantly: the exponent varies monotonically with the particle spin. It increases with the spin when the spin is parallel to the z-axis and decreases when the spin is antiparallel. Moreover, as the total angular momentum increases, the curves shift upward as a whole. Once the total angular momentum exceeds a certain threshold, the exponent surpasses the surface gravity, and the chaos bound is violated. A comparison of the $a>0$ and $a<0$ cases thus reveals that the particle spin, the total angular momentum, and the rotation direction of the black hole all affect the exponent, with retrograde black hole rotation playing a more pronounced role in triggering violations of the bound. In this comparison, the case $s=0$ serves as the spinless reference, corresponding to the geodesic limit discussed in Sec. 2. For $a>0$, the results with nonzero spin remain close to this reference value and stay below the surface gravity, indicating that the spin correction is not strong enough to violate the bound within the parameter range considered. For $a<0$, the deviation from the $s=0$ case becomes more pronounced as the total angular momentum increases, showing that the spin-curvature coupling can further modify the exponent beyond the effects of black hole rotation and particle angular momentum.

Figure 4 depicts the dependence of the exponents on the particle's total angular momentum. For $a>0$, the bound remains unviolated regardless of whether the spin is aligned with the z-axis, whereas for $a<0$, violations can occur. Specifically, the exponent increases monotonically with the angular momentum, implying that larger angular momentum leads to stronger chaos. The exponents vary more rapidly with angular momentum in the low-angular-momentum regime, and this rate of change gradually diminishes as the angular momentum increases. For $a<0$, when the spin is parallel to the z-axis, the exponents increase with the spin magnitude; when the spin



(a) $a<0.00$ (b) $a>0.00$

Fig. 1. (color online) The graph shows the variation of the effective potential of the neutral particle with radial coordinate, where $a=\pm 0.90$ is used.

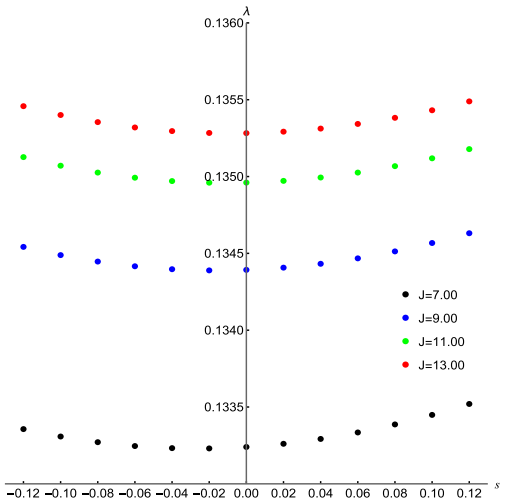


Fig. 2. (color online) The graph shows the variation in the LE of the particle's chaotic motion with respect to its spin, where $a = 0.90$ was used.

is antiparallel, the exponents decrease as the spin magnitude grows. Once the angular momentum exceeds a critical threshold, the bound is violated. For $a > 0$, the exponent increases with the spin magnitude irrespective of spin orientation. These results indicate that when the particle spin is parallel to the z-axis, a larger spin leads to more pronounced chaotic behavior.

From Fig. 5, we observe that for $a > 0$, no violation is detected within the explored parameter range, regardless of the spin value. In contrast, for $a < 0$, the gap between the exponents and the surface gravity narrows as the magnitude of the black hole angular momentum increases; once it exceeds a threshold, the gap becomes positive, signaling a violation of the bound. Notably, the insets of Fig. 5 show that when the spin is parallel to the z-axis, larger spin values shift the curves slightly upward, indicating that the spin magnitude has a mild enhancing effect on the exponent and can, to some extent, influence the critical condition for bound violation. These findings suggest that the black hole angular momentum plays the dominant role in governing the particle's chaotic behavior, while the particle spin only modulates the strength of chaos locally, without altering the overall trend.

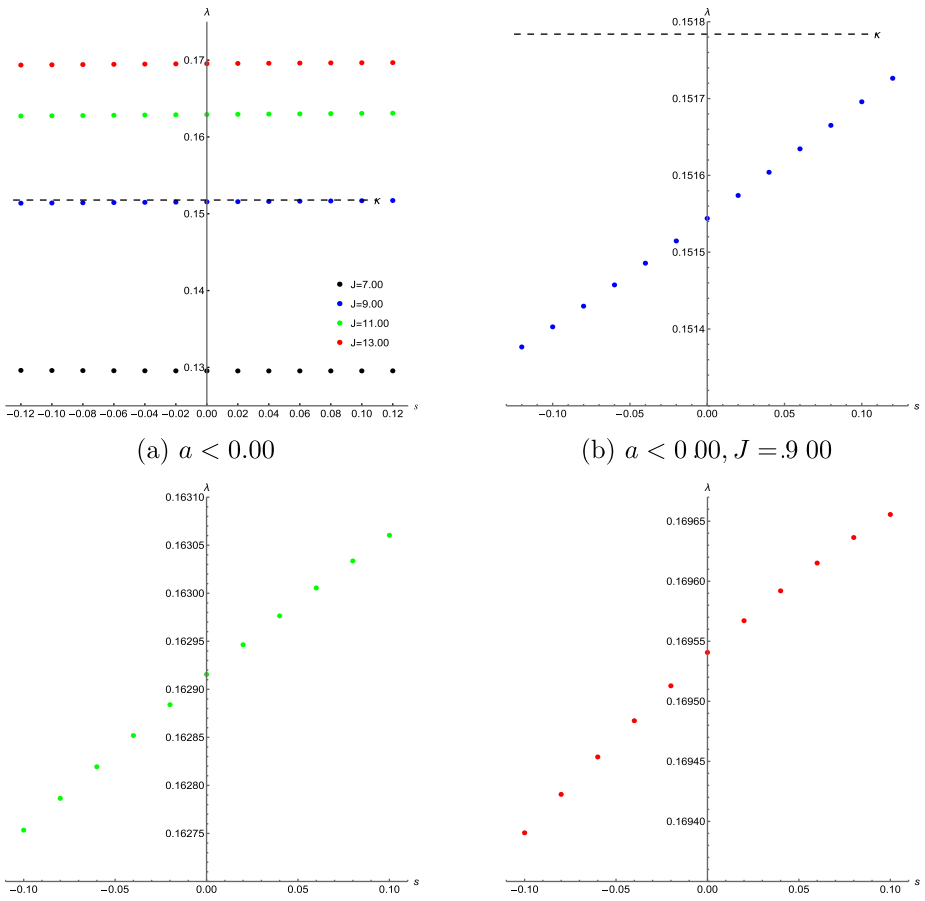
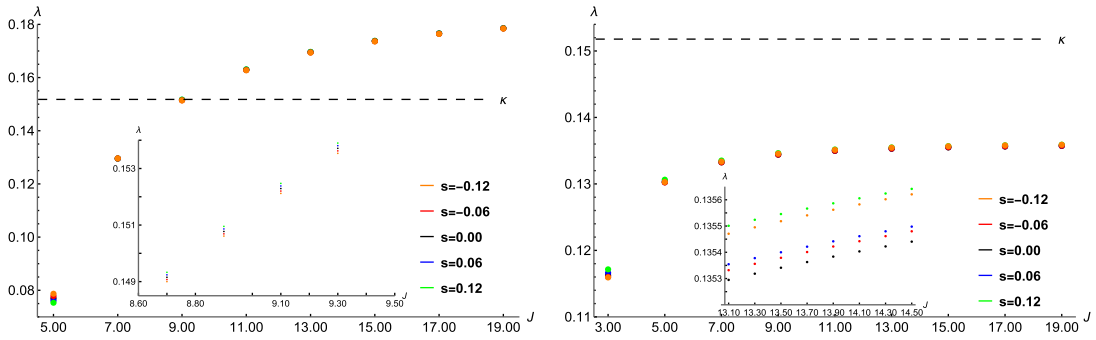


Fig. 3. (color online) The graph shows the variation in the LEs for the chaotic motion of the particle with respect to its spin, where $a = -0.90$ was used.



(a) $a < 0$ (b) $a > 0$

Fig. 4. (color online) The graph shows the variation in the LEs characterizing the particle's chaotic motion with respect to the total angular momentum, where $a = \pm 0.90$ was used.

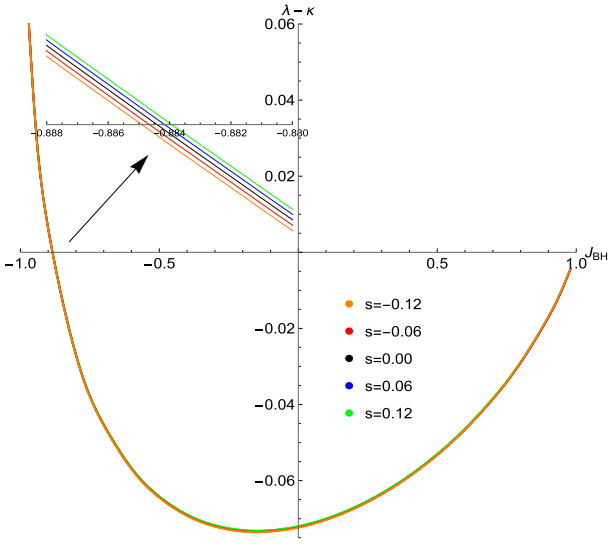


Fig. 5. (color online) The graph shows the variation in the LE with respect to the specific angular momentum of the Kerr black hole, for which $J = 10.00$ was used.

C. Chaos bound in extremal Kerr spacetime

In the preceding subsection, we analyzed the relationship between the exponents of spinning particles and the chaos bound in the background of a non-extremal Kerr black hole. For an extremal black hole, the inner and outer horizons coincide, and both the surface gravity and the Hawking temperature vanish; the corresponding system is therefore at zero temperature. The chaos bound reduces to

$$\lambda - \kappa = \lambda \leq 0. \tag{31}$$

Our purpose is to determine whether physically admissible unstable equilibrium orbits exist in the extremal Kerr background and to characterize their local radial instability. In this subsection, we investigate this bound by studying particle dynamics in such a zero-temperature system. In this case, the black hole rotational parameter can take only the values $+1$ or -1. As a quantitative validation of the spinless limit, we compare our extremal Kerr results with the known Kerr geodesic results reported in [25]. As shown in Fig. 6, our numerical calculations for $s = 0$ reproduce the same critical condition for the existence of unstable equilibrium orbits and yield behavior of the Lyapunov exponent consistent with respect to the particle angular momentum. This agreement confirms that the present formalism correctly recovers the known Kerr geodesic limit.

Using Eqs. (20)–(26) and Eq. (30), we compute the exponent and plot Figs. 7 and 8 to elucidate the influence of particle spin and total angular momentum on the exponent. For $M = 1$ and $a = 1$, no physically admissible unstable equilibrium orbit is found for the prograde configuration within the parameter range considered in this work.

Figure 7 shows the exponents as a function of particle spin. For all values of the spin and total angular momentum considered, the exponents are positive. When the

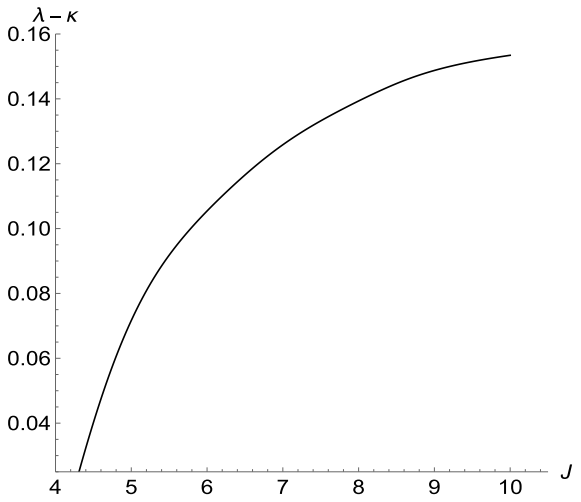
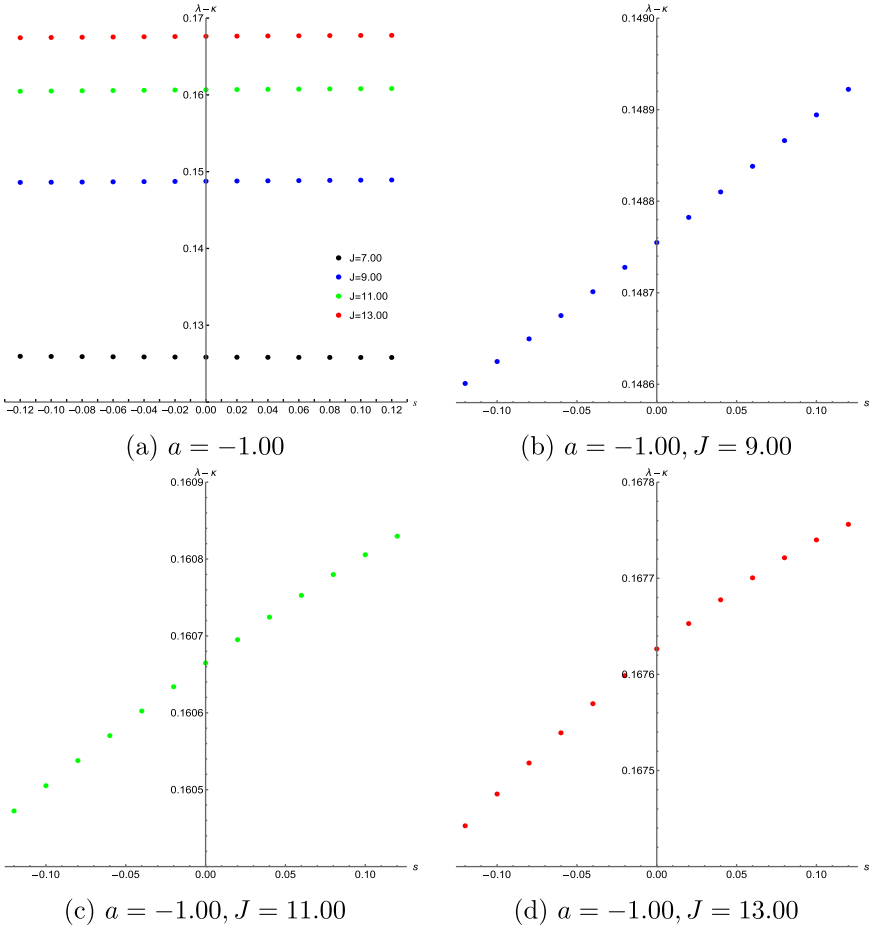


Fig. 6. Variation of the LE with the particle's total angular momentum J in the spinless limit, $s = 0$, for an extremal Kerr black hole.



(a) $a = -1.00$ (b) $a = -1.00, J = 9.00$

(c) $a = -1.00, J = 11.00$ (d) $a = -1.00, J = 13.00$

Fig. 7. (color online) The graph shows the variation of the LEs characterizing the particle's chaotic motion with respect to its spin in an extremal Kerr black hole.

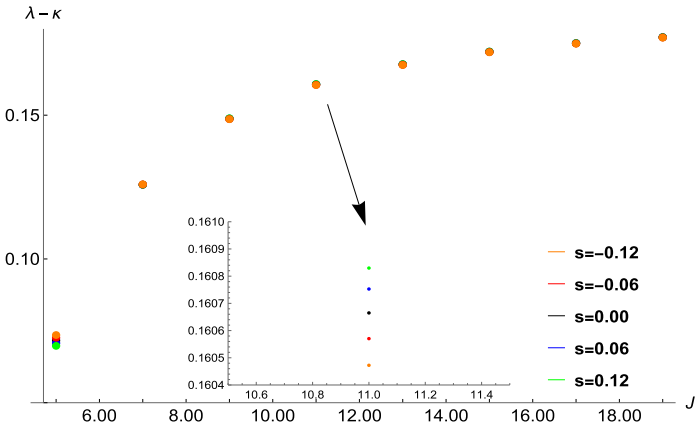


Fig. 8. (color online) The graph shows the variation in the LE associated with the particle's chaotic motion with respect to the total angular momentum in the extremal Kerr black hole.

spin is aligned with the z-axis, the exponents increase monotonically with spin magnitude. When it is anti-aligned, they decrease monotonically with increasing spin magnitude for all angular momenta.

Figure 8 shows the exponents as functions of the total angular momentum. For a fixed spin, the exponents increase monotonically with the total angular momentum, a trend also observed in the non-extremal case. For fixed total angular momentum, the exponents increase with increasing spin when the spin is aligned with the z-axis and decrease when it is anti-aligned. The curves corresponding to different spin magnitudes exhibit similar qualitat-

ive behavior and differ only quantitatively. These results indicate that, in the extremal case, positive exponents are obtained within the parameter ranges in which unstable equilibrium orbits exist.

IV. CONCLUSIONS AND DISCUSSIONS

In this work, we investigated the LEs characterizing the chaotic motion of neutral spinning particles around a Kerr black hole and tested the applicability of the chaos bound in this spacetime. In the non-extremal Kerr case, no violation of the bound is observed when the black hole rotation is aligned with the z-axis. When it is anti-aligned, violations occur only for specific ranges of the particle's total angular momentum, spin magnitude, and the black hole angular momentum. In the extremal case, where the surface gravity vanishes, the chaos bound reduces to $\lambda \leq 0$. For the parameter ranges in which physically allowed unstable equilibrium orbits exist, all exponents are positive. It should be noted, however, that when $M = a = 1$, the effective potential has no local maximum, and consequently no unstable orbit exists. Therefore, within the physically allowed orbital regimes considered here, positive exponents are obtained whenever unstable equilibrium orbits exist. We also examined the spinless limit $s = 0$, in which the radial equation reduces to the standard geodesic motion of a spinless massive particle in Kerr spacetime. This limiting case provides a reference for identifying the influence of spin-curvature coupling on the exponent.

The location of the particle's unstable equilibrium orbit depends on the black hole angular momentum, the particle's spin magnitude, and its total angular momentum. Varying these parameters shifts the equilibrium orbit, which in turn modifies the exponents. It is important to note that the particle's total angular momentum and spin are not freely adjustable; rather, they are uniquely determined by the detailed orbital dynamics around the black hole. In our analysis, when the total angular momentum is varied, the equilibrium orbit changes accordingly, so the orbit is a function of the angular momentum. By contrast, in [55], the authors vary the equilibrium orbit, and the angular momentum changes in response; hence, in that work, the angular momentum is treated as a function of the orbit. For computational simplicity, we set the black hole mass $M = 1$ and express all particle quantities in normalized form. This choice fixes the length scale of the system and does not affect the test-particle condition $m/M \ll 1$. The backreaction of the spinning particle on the Kerr geometry has been neglected. Therefore, a definitive confirmation of a violation of the chaos bound will require incorporating these effects in future analyses.

References

[1] S. H. Shenker and D. Stanford, JHEP **12**, 046 (2014)
[2] D. A. Roberts and D. Stanford, JHEP **03**, 051 (2015)
[3] A. Kitaev, talk at Stanford SITP seminars, Nov. 11, (2014)
[4] A. Kitaev, talk at Stanford SITP seminars, Dec. 18, (2014)
[5] J. Maldacena, S. H. Shenker, and D. Stanford, JHEP **08**, 106 (2016)
[6] A. L. Fitzpatrick and J. Kaplan, JHEP **05**, 070 (2016)
[7] W. H. Huang, Phys. Rev. D **97**, 066020 (2018)
[8] Y. Ling and Z. Y. Xian, JHEP **09**, 003 (2017)
[9] A. A. Patel and S. Sachdev, Proc. Nat. Acad. Sci. **114**, 1844 (2017)
[10] G. J. Turiaci, JHEP **07**, 099 (2019)
[11] M. Blake and R. A. Davison, JHEP **01**, 013 (2022)
[12] A. Addazi, S. Capozziello, and S.D. Odintsov, Phys. Lett. B **816**, 136257 (2021)
[13] S. H. Shenker and D. Stanford, JHEP **03**, 067 (2014)
[14] S. Sachdev and J. Ye, Phys. Rev. Lett. **70**, 3339 (1993)
[15] A. Kitaev and S. J. Suh, JHEP **05**, 183 (2018)
[16] J. Polchinski and V. Rosenhaus, JHEP **1604**, 001 (2016)
[17] J. Maldacena and D. Stanford, Phys. Rev. D **94**, 106002 (2016)
[18] K. Hashimoto and N. Tanahashi, Phys. Rev. D **95**, 024007 (2017)
[19] Q. Q. Zhao, Y. Z. Li, and H. Lü, Phys. Rev. D **98**, 124001 (2018)
[20] Y. Q. Lei and X. H. Ge, Phys. Rev. D **105**, 084011 (2022)
[21] Y. Q. Lei, X. H. Ge, and C. Ran, Phys. Rev. D **104**, 046020 (2021)
[22] Y. Q. Lei and X. H. Ge, Phys. Rev. D **107**, 106002 (2023)
[23] Y. Q. Lei and X. H. Ge, Phys. Lett. B **856**, 138929 (2024)
[24] C. H. Gao, D. Y. Chen, C. Y. Yu *et al*., Phys. Lett. B **833**, 137343 (2022)
[25] N. Kan and B. Gwak, Phys. Rev. D **105**, 026006 (2022)
[26] B. Gwak, N. Kan, and B. H. Lee, JHEP **09**, 026 (2022)
[27] J. Park and B. Gwak, JHEP **04**, 023 (2024)
[28] B. Singh, N. Padhi, and R. R. Nayak, Eur. Phys. J. C **85**, 570 (2025)
[29] H. Lee and B. Gwak, Phys. Rev. D **112**, 046018 (2025)
[30] K. Hashimoto and K. Sugiura, Phys. Rev. D **107**, 066005 (2023)
[31] J. Y. Xie, J. Wang, and B. Tang, Phys. Dark. Univ **42**, 101271 (2023)
[32] S. Jeong, B. H. Lee, H. Lee *et al*., Phys. Rev. D **107**, 104037 (2023)
[33] P. Dutta, K. L. Panigrahi, and B. Singh, JHEP **02**, 043 (2025)
[34] K. Li, D. Z. Ma, and Z. M. Xu, Phys. Lett. B **860**, 139164 (2025)
[35] A. Fayyaz, G. Abbas, M. B. Asfour *et al*., Phys. Lett. B **871**, 139965 (2025)
[36] M. Y. Wang, S. W. Li, D. F. Hou *et al*., arXiv: 2601.22549v1
[37] C. Yang, D. Y. Chen, and Y. T. Liu, JHEP **04**, 205 (2026)
[38] X. W. Li, B. B. Chen, and G. P. Li, arXiv: 2604.03914
[39] R. Hojman and S. Hojman, Phys. Rev. D **15**, 2724 (1977)
[40] W. Tulczyjew, Acta Physica Polonica **18**, 393 (1959)

[41] A.J. Hanson and T. Regge, Ann. Phys. **87**, 498 (1974)
[42] O. Y. Tsupko, G. S. Bisnovatyi-Kogan, and P.I. Jefremov, Grav. Cosmol **22**, 138 (2016)
[43] O. Semerak, Mon. Not. Roy. Astron. Soc. **308**, 863 (1999)
[44] M. D. Hartl, Phys. Rev. D **67**, 024005 (2003)
[45] D. Bini, F. D. Felice, and A. Geralico, Class. Quant. Grav. **21**, 5441 (2004)
[46] K. Kyrian and O. Semerak, Mon. Not. Roy. Astron. Soc. **382**, 1922 (2007)
[47] W. B. Han, Gen. Rel. Grav. **40**, 1831 (2008)
[48] M. Favata, Phys. Rev. D **83**, 024028 (2011)
[49] M. Saijo, K. Maeda, M. Shibata *et al*., Phys. Rev. D **58**, 064005 (1998)
[50] M. Y. Guo and S. J. Gao, Phys. Rev. D **93**, 084025 (2016)
[51] R. M. Wald, Phys. Rev. D **6**, 406 (1972)
[52] P. I. Jefremov, O. Y. Tsupko, and G. S. B. Kogan, Phys. Rev. D **91**, 124030 (2015)
[53] V. Cardoso, A. S. Miranda, E. Berti *et al*., Phys. Rev. D **79**, 064016 (2009)
[54] S. Y. Ciou, T. Hsieh, and D. S. Lee, JCAP **05**, 086 (2025)
[55] T. V. Targema, K. Bamba, and U. Zafar, Phys. Rev. D **113**, 104056 (2026)